Plasmonic Hybridization between Nanowires and a Metallic Surface: A Transformation Optics Approach

Alexandre Aubry,[†,*] Dang Yuan Lei, Stefan A. Maier, and John B. Pendry

The Blackett Laboratory, Department of Physics, Imperial College London, London SW7 2AZ. [†] Present address: Institut Langevin, ESPCI ParisTech, CNRS UMR 7587, 10 rue Vauquelin, 75231 Paris Cedex 05, France.

ABSTRACT The interaction between metallic nanowires and a metal substrate is investigated by means of transformation optics. This plasmonic system is of particular interest for single molecule detection or nanolasers. By mapping such a plasmonic device onto a metal−insulator−metal infinite structure, its optical response can be fully derived analytically. In this article, the absorption cross-section of a nanowire placed close to a metallic surface is derived within and beyond the quasi-static limit. The system is shown to support several modes characterized by a different angular momentum and whose resonance red-shifts when the nanoparticle approaches the metal substrate. These resonances give rise to a drastic field enhancement (>10^2) within the narrow gap separating the nanoparticle from the metal surface. The case of a nanowire dimer is also investigated and is closely related to the previous configuration. More physical insights are provided especially with respect to the invisibility dips appearing in the radiative spectrum. Numerical simulations have also been performed to confirm our analytical predictions and determine their range of validity.

KEYWORDS: plasmonics · nanoparticles · transformation optics · field enhancement · hybridization · metal surface · invisibility dips

Surface plasmons have drawn considerable attention for the past decade because of their ability to route and manipulate light at the nanoscale.[1−4] Squeezing light into nanoscale volumes greatly boosts light−matter interactions as shown by surface-enhanced Raman scattering (SERS),[5,6] enhanced fluorescent emission,[7,8] or high harmonic generation experiments.[9] There have been tremendous efforts to design and optimize nanostructures in order to obtain the best efficiency in light harvesting and nanofocusing. Until now, this optimization has mainly relied on numerical simulations.[10,11] The latter ones are useful but quite misleading since they somehow fail to highlight the physics hidden behind the calculations. Recently, a more powerful approach based on transformation optics has been proposed to derive analytically the optical response of complex nanostructures.[12] It consists in finding a conformal map that transforms the plasmonic nanostructure under investigation into a simpler plasmonic system that can be solved analytically. Transformation optics closely links the physics at work in each of the different geometries and gives a unique physical insight on the propagation of surface plasmons in complex nanostructures. In a recent letter,[13] this strategy has been applied to the interaction between nanoparticles. Some results of the analytical calculations have been presented to analyze the spatial and spectral properties of the field enhancement in the gap separating two nanoparticles. However, no analytical proof has been provided. In this article, the corresponding theory is derived in details and more physical insights are provided especially with respect to the invisibility dips appearing in the scattering spectrum.[13] Note that several experimental works have dealt recently with metallic nanowires (see *e.g.*, refs 14 and 15). The case of a nanowire or a nanosphere placed in the vicinity of a metal plate has also drawn a great deal of attention in plasmonics whether it be for nanolaser applications[16] or SERS experiments.[17] Consequently, this configuration will be addressed in this paper and shown to be closely related to the dimer case.

The localized surface plasmon (LSP) resonances supported by coupled nanoparticles were first introduced by Bergman[18−20] and then by McPhedran using conformal mapping[21,22] in the context of effective medium theory, 30 years ago. This topic was then resuscitated by the emergence of plasmonics in the past decade. Whereas an isolated nanoparticle only exhibits a single dipole resonance around the surface plasmon frequency, several resonances may arise in the visible/near-infrared spectra for dimers[23−31] and lead to a drastic field enhancement in the narrow gap separating the two nanoparticles.[32−35] An elegant physical picture to describe this interaction is the plasmon hybridization model proposed by Peter Nordlan

* Address correspondence to a.aubry@imperial.ac.uk.

Received for review February 2, 2011 and accepted March 1, 2011.

Published online March 01, 2011
10.1021/nn200438e

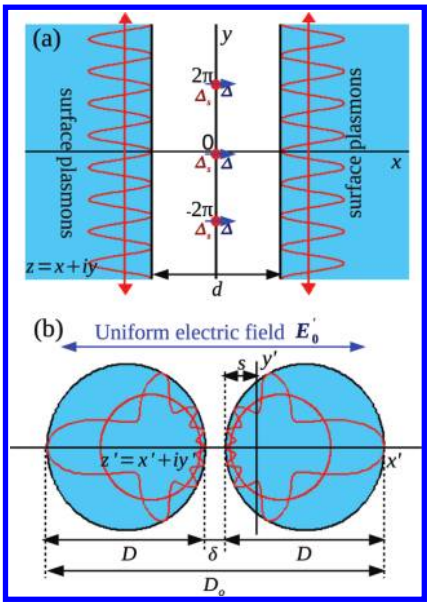

Figure 1. (a) Two semi-infinite metallic slabs separated by a thin dielectric film support surface plasmons that couple to an array of dipoles $\hat{\Delta}$ (blue arrows). The array pitch is 2π. An array of absorbing particles is superimposed to the dipole sources to take into account the radiative damping. (b) The transformed material of panel a is a pair of cylinders of diameter *D*, separated by a narrow gap δ. The dipole sources $\hat{\Delta}$ are transformed into a uniform electric field E_0'.

der and colleagues, a few years ago.[36−40] However, this model still demands numerical simulations to obtain the optical response of nanostructures. On the contrary, transformation optics provides an elegant and powerful tool to solve analytically complex plasmonics problems.[12,41−45] By applying a conformal transformation that we will describe, a nanowire dimer can be transformed into a system consisting of an array of dipoles sandwiched between two semi-infinite metal slabs (see Figure 1). The slab problem can be easily solved analytically under the electrostatic approximation. Then, by conformal mapping, the behavior of LSPs and their coupling with the external field are deduced in the transformed geometry. This problem can be decomposed as a sum of modes denoted by a discrete angular momentum *n* in agreement with the hybridization picture.[13] The absorption cross-section and the electric field distribution in the near-field of the nanowires are expressed analytically. These theoretical results are compared to numerical simulations and a perfect agreement is found for structure dimensions up to 20 nm.

Our theory is then extended beyond the quasi-static limit by considering radiative damping.[46] The scattering spectrum of the dimer displays some *invisibility* dips resulting from the destructive interference between the modes supported by the dimer. In this article, we investigate the electric field distribution associated to these invisibility dips and show that the interference between each mode is constructive in the near-field, albeit destructive in the far-field. Taking into account radiation damping also allows the derivation of new analytical expressions for the scattering and absorption cross sections, as well as for the field enhancement. These theoretical results are compared to numerical simulations, and a nice agreement is found for structure dimension up to 100 nm. Considering a gap of 0.5 nm as being the limit for quantum mechanical effects[47] and a nanowire diameter of 10 nm as being the limit for neglecting nonlocal effects,[48] the maximum field enhancement that may be induced by the nanowire dimer is found to be of the order of 200 within a classical approach.

In the second part of this paper, the plasmonic structure consisting of a nanowire placed on top of a metal substrate is investigated and shown to be strongly related to the dimer case. The hybridization between the surface plasmon propagating along the metal plate and the localized surface plasmon supported by the nanowire leads to the occurrence of several resonances in the visible spectrum. A strong field enhancement is expected within the narrow layer separating the nanowire and the metal plate at the corresponding resonant frequencies. The originality of this configuration consists first in solving this problem with a quasi-static approach whereas the metal plate is semi-infinite. However, as the field is extremely confined in the narrow gap separating the nanoparticle and the metal substrate, our approach is valid as long as the nanowire is small compared to the wavelength (of diameter $D < 100$ nm). This will be confirmed by numerical simulations. Second, a half plane-wave illumination of the system is considered due to the infiniteness of the metal substrate. This will require a refining of the theory compared to the first part of the article and previous works. The absorption cross-section of the nanowire as well as the field enhancement induced by the system are both derived theoretically and show a remarkable agreement with numerical simulations for nanowire diameter up to 100 nm. In this configuration, the nanowire benefits from the presence of the metal plate to harvest light more efficiently and induce strong field enhancements ($>10^2$). This configuration is thus an excellent candidate for single molecule detection as already pointed out in past studies.[17,49]

RESULTS AND DISCUSSIONS

Plasmonic Interaction between Two Nanowires. The plasmonic interaction between two nanowires is addressed in this section. First, the conformal transformation mapping the nanowire dimer problem onto a slab geometry is presented (Figure 1). The solution of the slab problem allows an analytical derivation of the absorption cross-section and the electric field distribution under the quasi-static approximation. Following a strategy presented in ref 46, the radiation damping is then taken into account by introducing fictive absorbing particles in the slab geometry.

Conformal Transformation. Our canonical system is an array of dipoles oriented along the *x*-axis and aligned along the *y*-axis, with a pitch of 2π, located in a thin slab of insulator of thickness *d* surrounded by two semi-infinite metal slabs (Figure 1a). Now apply the following conformal transformation,

$$z' = \frac{g}{\exp(z) - 1} \quad (1)$$

$z = x + iy$ and $z' = x' + iy'$ are the usual complex number notations in the original and transformed frames, respectively; *g* is an arbitrary constant. The transformed material consists of a pair of nanowires separated by a narrow gap (see Figure 1b).The diameter of the two cylinders is given by

$$D = \frac{g}{\sinh(d/2)} \quad (2)$$

The distance δ separating the two cylinders can be expressed as

$$\delta = g \tanh(d/4) \quad (3)$$

We also define a key parameter,

$$\rho = \frac{\delta}{2D} = \sinh^2(d/4) \quad (4)$$

which is the ratio between the gap δ separating the two cylinders and two times their diameter, 2*D*. All the physical quantities that we will derive in this section (absorption and scattering cross sections, field enhancement) will be expressed as a function of this ratio ρ and of the cylinder diameter *D*. From eq 2−4, we can express *g* and *d* as a function of ρ and *D*:

$$g = 2D\sqrt{\rho(1+\rho)} \quad (5)$$

$$d = 4 \ln(\sqrt{\rho} + \sqrt{1+\rho}) \quad (6)$$

These last expressions will be useful when we will deduce from the slab problem the solution in the transformed geometry. The shift *s* between the axis *y*′ and the surface of the cylinder (see Figure 1b) is given by

$$s = \frac{g}{(1+e^{d/2})} = \frac{2D\sqrt{\rho(1+\rho)}}{1+(\sqrt{\rho}+\sqrt{1+\rho})^2} \quad (7)$$

At last, the overall physical cross-section D_o of the nanowire dimer can be expressed as

$$D_o = 2D + \delta = 2D(1+\rho) \quad (8)$$

Transformation of the sources is also shown in Figure 1. The original dipoles $\hat{\Delta}$ are transformed into a uniform electric field,

$$\mathbf{E}_0' = \frac{\hat{\Delta}}{2\pi\varepsilon_0 g} \quad (9)$$

Note that we made the choice of an electric field $\mathbf{E}_0'$ polarized along *x*′ since $\hat{\Delta}$ is assumed to be aligned along *x*. Actually, this polarization is by far more efficient to excite surface plasmon modes than a transverse polarization (along *y*′).[12] In a first step, we will assume that the cylinder pair is sufficiently small such that the surface plasmon modes are well described in the quasi-static approximation. The uniform electric field $\mathbf{E}_0'$ can then be considered as due to an incident plane wave. Furthermore, in this case, the dielectric properties of the nanostructure are the same as those of the slab from which it is derived. Also preserved under the transformation is the electrostatic potential:

$$\phi(x, y) = \phi'(x', y') \quad (10)$$

Hence, solving the relatively tractable slab problem (Figure 1a) solves the dimer problem (Figure 1b). The electrostatic potential in the slab geometry is derived in the Methods section (eqs 55−57).

Light Harvesting in the Quasi-static Limit. As shown in previous works,[42,43,46] dipoles and fields exchange their role in the two frames: the emitting dipole $\hat{\Delta}$ in the slab geometry is transformed into a uniform incident field $\mathbf{E}_0'$ (eq 9), whereas the backscattered electric field at the dipole location, $\mathbf{E}(z = 0)$, directly provides the dipole moment **p** of the nanostructure in the transformed frame,

$$\mathbf{p} = 2\pi\varepsilon_0 g \mathbf{E}(z = 0) \quad (11)$$

The energy dissipation is thus the same in the original and transformed frames. Hence, by computing the dipole power dissipated in the slab geometry, one can deduce the power absorbed by the nanowires in the dimer geometry.

Let us compute the energy dissipated in the original frame. From the expression of the induced potential ϕ for $|x| < d/2$ derived in the Methods section (eq 55), we can deduce the electric field at the dipoles

$$\mathbf{E}(z = 0) = -\nabla\phi(z = 0) = -\frac{\hat{\Delta}}{\pi\varepsilon_0}\beta \quad (12)$$

with

$$\beta = \frac{\varepsilon - 1}{\varepsilon + 1} \sum_{n=1}^{+\infty} \frac{n}{e^{nd} - \frac{\varepsilon - 1}{\varepsilon + 1}} \quad (13)$$

The dissipated power, P_a, can then be deduced from this backscattered electric field:

$$P_a = -\frac{\omega}{2} \mathrm{Im}\{\hat{\Delta}^* \cdot \mathbf{E}(z = 0)\} \quad (14)$$

If we inject the expression of $\mathbf{E}(z = 0)$ (eq 12) into the last equation, replace *g*, *d*, and $\hat{\Delta}$ by their expressions (eqs 5,6, and 9) and renormalize P_a by the incoming flux $P_{in} = \varepsilon_0 c_0 |\mathbf{E}_0'|^2/2$, we can derive the absorption cross-section $\sigma_a^o = P_a/P_{in}$ of the cylinder pair under the

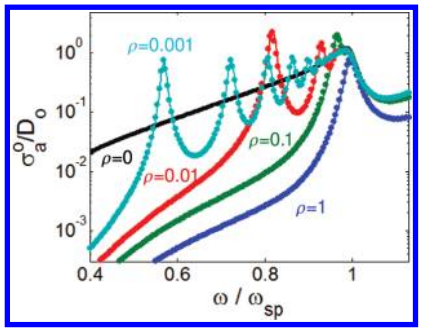

Figure 2. Absorption cross-section σ_a^o normalized by the physical cross-section D_o as a function of frequency for different values of $\rho = 10^0, 10^{-1}, 10^{-2}, 10^{-3}$, with $D_o = 20$ nm. The quasi-static theoretical predictions (continuous lines, eq 15) are compared to numerical simulations (dots). The case of kissing cylinders ($\rho = 0$, black continuous line) is also shown for comparison.[12,42] The metal is assumed to be silver with a surface plasmon frequency $\omega_{sp} = 3.67$ eV and permittivity taken from Johnson and Christy[50].

electrostatic approximation,

$$\sigma_a^o = 16\pi k_0 \rho(1+\rho)D^2 \times \mathrm{Im}\left\{\frac{\varepsilon-1}{\varepsilon+1}\sum_{n=1}^{+\infty}\frac{n}{(\sqrt{\rho}+\sqrt{1+\rho})^{4n}} - \frac{\varepsilon-1}{\varepsilon+1}\right\} \quad (15)$$

where the superscript o accounts for the quasi-static approximation and $k_0 = \omega/c_0$ is the wavenumber in vacuum. Note that, rigorously, this expression corresponds to the extinction cross-section. However, as radiation losses are neglected under the quasi-static approximation, this quantity is here strictly equivalent to the absorption cross-section. σ_a^o scales as the square of the diameter D of the cylinders, which is typical of a 2D configuration. The absorption cross-section is the sum of each contribution due to the surface plasmon modes supported by the cylinder pair and denoted by their angular moment n. Each mode may give rise to a resonance at a frequency satisfying the following relation

$$(\sqrt{\rho}+\sqrt{1+\rho})^{4n} = \mathrm{Re}\left\{\frac{\varepsilon-1}{\varepsilon+1}\right\} \quad (16)$$

Note that this condition of resonance only depends on the ratio ρ between the gap separating the nanoparticles and two times their diameters (eq 4).

Figure 2 illustrates this resonant feature by displaying σ_a^o/D_o as a function of frequency for different values of ρ and for an overall physical cross-section $D_o = 20$ nm. For this figure as well as in the following of the study, the metal is assumed to be silver with a surface plasmon frequency $\omega_{sp} = 3.67$ eV and permittivity taken from Johnson and Christy.[50] Our theoretical predictions are compared to numerical simulations performed with the software Comsol. The perfect agreement between theoretical and numerical curves shows how our theory can accurately predict the optical response of nanowire dimers in the quasi-static limit.

As shown in Figure 2 and as already discussed in ref 13, the absorption spectrum is strongly dependent on the gap separating the two nanoparticles. In the strong coupling regime, several resonances associated to small angular momenta n start to arise at a smaller frequency than ω_{sp} and tend to red-shift when the two nanoparticles approach each other.[13] When a resonance occurs, the cylinder pair constitutes a powerful light harvesting device for an incident wave polarized along x' (see Figure 2). Even for such a small particle size ($D_o = 20$ nm), the absorption cross-section can be superior to the physical cross-section. For constant ratio ρ, σ_a/D_o scales linearly with D_o. Thus higher cross sections could be obtained for larger cylinders, but in this case our near field analytic theory may not be valid as we will see in the following. On the contrary, the device does not exhibit any multi-resonant feature if the incident wave is polarized along y' (results not shown here). Only one peak is observed around $\omega = \omega_{sp}$ due to the individual resonance of each nanowire. This fact has already been pointed out in previous numerical studies.[24]

Nanofocusing in the Quasi-static Limit. Now that the light harvesting properties of the nanowires have been studied under the quasi-static approximation, we now focus on the electric field induced in the near-field of the dimer. Each of the resonances pointed out previously is associated to a particular distribution of the electric field. The nanowire dimer is shown to lead to a strong far-field to near-field conversion of energy: a considerable confinement and amplification of the electric field can be found in the narrow gap separating the two nanoparticles.

Under the conformal transformation, the potential is preserved (eq 10). The electric field $\mathbf{E}'(x',y')$ in the transformed geometry can then be easily deduced from the potential,

$$\mathbf{E}'_{x'} = -\frac{\partial\phi'}{\partial z'}\frac{\partial z}{\partial x'} - \frac{\partial\phi'}{\partial z'^*}\frac{\partial z'^*}{\partial x'} = -\frac{\partial\phi'}{\partial z'} - \frac{\partial\phi'}{\partial z'^*} \quad (17)$$

$$\mathbf{E}'_{y'} = -\frac{\partial\phi'}{\partial z'}\frac{\partial z}{\partial y'} - \frac{\partial\phi'}{\partial z'^*}\frac{\partial z'^*}{\partial y'} = -\mathrm{i}\frac{\partial\phi'}{\partial z'} + \mathrm{i}\frac{\partial\phi'}{\partial z'^*} \quad (18)$$

The expression of the potential ϕ derived in the Methods section (eqs 55−57) can be injected into the last equation. It turns out that the electric field can be decomposed as an infinite sum of modes,

$$\mathbf{E}' = \sum_{n=1}^{\infty}\Psi^{(n)} \quad (19)$$

The analytical expression of the modes $\Psi^{(n)}$ is derived in the Methods section (eqs 58−63). Note that in the near field approximation, the enhancement of electric field is independent of the size of the system.

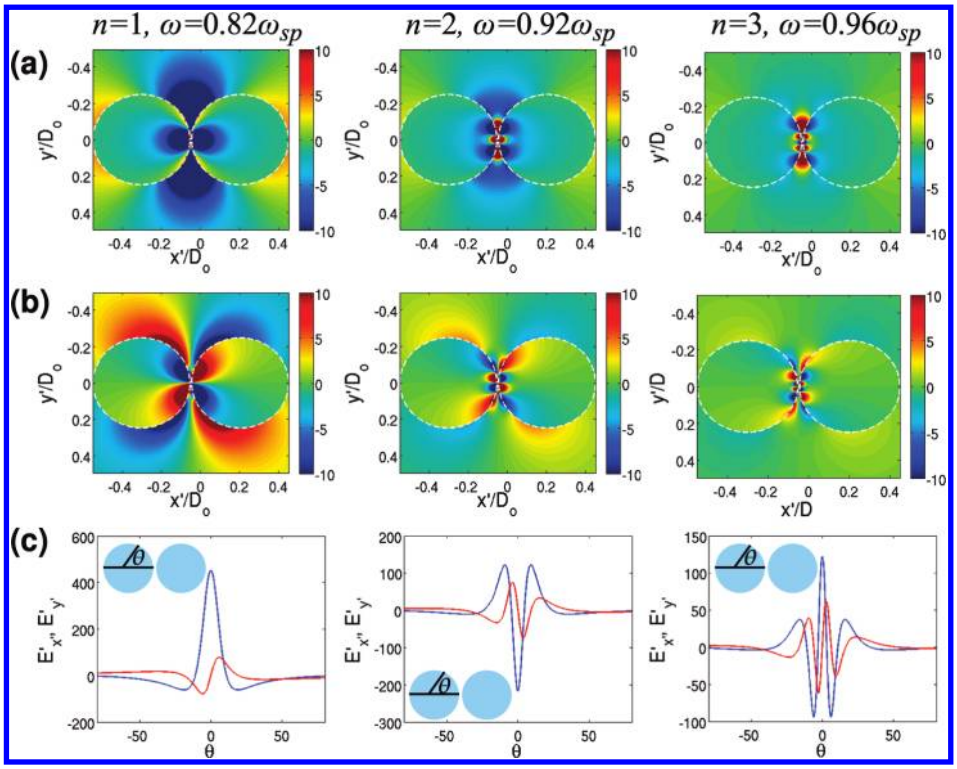

Figure 3. Electric field for $\rho = 0.01$ associated with the modes $n = 1,2,3$ (from left to right) at their corresponding resonant frequencies (eq 16). (a) Amplitude of the imaginary part of $\psi_x^{(n)}$ normalized by the incoming field E_0' (polarized along x'). (b) Amplitude of the imaginary part of $\psi_y^{(n)}$ normalized by the incoming field E_0' (polarized along x'). For a and b plots, the color scale is restricted to [−10 10] but note that the field magnitude can be far larger in the narrow gap between the structures. (c) Amplitude of the imaginary part of $\psi_x^{(n)}/E_0'$ (blue) and $\psi_y^{(n)}/E_0'$ (red) along the cylinder surface as a function of the angle θ defined in the figure.

Figure 3 shows the result of our analytical calculation of the first three modes taken at their resonant frequencies (eq 16). The gap δ is fixed to $D/50$ ($\rho = 0.01$). The metal is assumed to be silver with permittivity taken from Johnson and Christy.[50] Figure 3 plots a and b represent the imaginary part of the field distribution along x' and y', respectively. These figures can be easily interpreted with conformal transformation. In the slab frame, the surface plasmon modes transport the energy of the dipoles along the surface of the metal slabs (see Figure 1). The same modes are excited in the transformed frame and propagate along the cylinder surface. As they approach the gap separating the two nanoparticles, the LSPs supported by each nanoparticle couple to each other, their wavelength shortens, and group velocity decreases in proportion. This leads to an enhancement of the field in the narrow gap. However, contrary to the kissing cylinders,[12] the velocity of LSPs does not vanish, and energy cannot accumulate infinitely in the narrow gap. Instead, LSPs propagate indefinitely around the cylinders, leading to the resonant behavior pointed out previously.

Figure 3c represents the imaginary part of the field along the surface of the cylinders. The comparison between each mode allows the confirmation of our previous qualitative description: the angular momentum n associated to each mode corresponds to the number of spatial periods covered by the surface plasmon when propagating around one nanowire. Figure 3c also highlights the drastic field enhancement that can be induced within the gap between the two nanoparticles. Typically, for $\delta = D/50$, the field enhancement $|E'|/E_0$ can reach a value of 600. Note that the field enhancement is less than 1 order of magnitude of the value obtained for kissing cylinders ($\sim 10^4$).[12,42]

Scattering Spectrum and Invisibility Dips. A recent article[46] has shown how the radiative losses in the transformed frame can be mapped directly onto a fictive absorbing particle in the original geometry. This can be done by considering the scattered field $\mathbf{E}_s'$ in the near-field of the nanostructure. In free space, if we neglect the real part of the dyadic Green function linking the dipole moment to the scattered field, $\mathbf{E}_s'$ is given by[46]

$$\mathbf{E}'_s = -i\frac{{k_o}^2}{8\varepsilon_o}\mathbf{p} \qquad (20)$$

The scattered field is uniform in the near field of the nanoparticle and its counterpart in the slab geometry corresponds to an array of dipoles, $\hat{\Delta}_s = 2\pi\varepsilon_0 g\mathbf{E}_s'$, superimposed to the original dipoles $\hat{\Delta}$ (Figure 1). Replacing $\mathbf{E}_s'$ by its expression in (eq 20) and the dipole moment $\mathbf{p}$ by (eq 11) yields the following expression for $\hat{\Delta}_s$,

$$\hat{\Delta}_s = -i\frac{\pi^2}{2}\varepsilon_o g^2 {k_o}^2 \mathbf{E}(z = 0) \qquad (21)$$

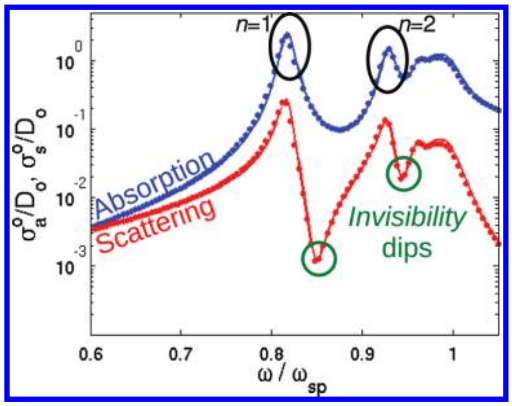

Figure 4. Scattering (in red) and absorption (in blue) cross sections, σ_s^o and σ_a^o, normalized by the overall physical cross-section D_o = 20 nm, as a function of frequency for ρ = 0.01. The quasi-static theoretical predictions (continuous lines, eq 15 and eq 23) are compared to the results of numerical simulations (dots).

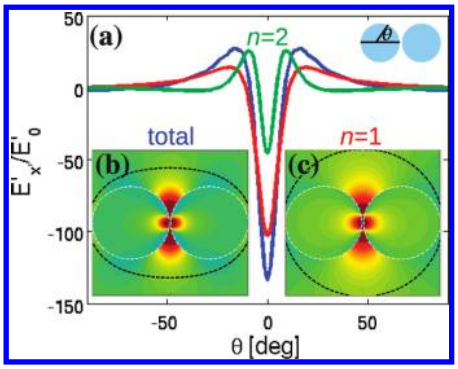

Figure 5. The main panel (a) represents the real part of $E'_{x'}/E'_0$ (blue) and the respective contributions of the first mode (red) and of the second mode (green) along the surface of the nanowire as a function of θ, for ρ = 0.01. These plots are made at the first invisibility dip ($\omega = 0.85\omega_{sp}$, see Figure 4). The two subpanels represent the corresponding field distributions: $E'_{x'}/E'_0$ (b) and $\psi_{x'}^{(1)}/E'_0$ (c). For both subpanels, the black dashed line surrounds the area of amplification of the field, that is, the region for which $|E'|/E'_0 > 1$ and $|\Psi^{(1)}|/E'_0 > 1$, respectively. The color scale is linear and restricted to [−10;10], but note that the field is by far larger within the narrow gap.

The strength of these dipoles $\hat{\Delta}_s$ is directly proportional to the incident field $\mathbf{E}(z = 0)$. Hence they correspond to small absorbing particles of polarizability $\gamma_s = -i(\pi^2/2)\varepsilon_o g^2 k_o^2$, accounting for the radiative losses in the transformed geometry.

The power radiated by the nanostructure is equivalent to the power absorbed by these fictive adsorbing particles in the slab frame,

$$P_s = -\frac{\omega}{2}\mathrm{Im}\{\gamma_s\}|\mathbf{E}(z = 0)|^2 \qquad (22)$$

If we inject the expressions of $\mathbf{E}(z = 0)$ (eq 12), γ_s (eq 21), and g (eq 5) into the last equation and normalize it by the incoming flux $P_{in} = \varepsilon_0 c_0 |\mathbf{E}'_0|^2/2$, the scattering cross-section σ_s^o of the nanowire dimer can be deduced in the quasi-static limit,

$$\sigma_s^o = 32\pi^2 k_o^3 \rho^2 (1+\rho)^2 D^4 \times \left| \frac{\varepsilon - 1}{\varepsilon + 1} \sum_{n=1}^{+\infty} \frac{n}{(\sqrt{\rho}+\sqrt{1+\rho})^{4n}} - \frac{\varepsilon - 1}{\varepsilon + 1} \right|^2 \qquad (23)$$

The radiative spectrum exhibits the same resonant feature as observed previously for the absorption spectrum (eq 16). Figure 4 illustrates this fact by showing the absorption and scattering cross sections for ρ = 0.01 and D_o = 20 nm. As already pointed out in ref 13, the resonances displayed by the scattering cross-section clearly exhibit an asymmetric lineshape. We stress on the fact that these are not Fano resonances which correspond usually to the coupling between bright and dark modes and manifest themselves in the extinction spectrum.[51−54] The sharp dips in the radiative spectrum are due here to the destructive interference between each successive bright mode. Typically, the sharp dip observed at $\omega = 0.85\omega_p$ in Figure 4 results from the destructive interference between the modes n = 1 and n = 2 which resonate on each side of the dip. This feature can be promising in the perspective of sensing applications, since the ratio between the absorption and scattering cross sections can reach for instance a value of 150 in the conditions considered in Figure 4 (ρ = 0.01, D_o = 20 nm).

Figure 5 shows the electric field distribution associated with these invisibility dips. Figure 5a represents the field along one of the nanowire plotted as a function of θ at the first invisibility dip frequency for ρ = 0.01 (*i.e.*, at $\omega = 0.85\omega_{sp}$, see Figure 4). The real part of the total electric field along the x'-direction, $E'_{x'}/E'_0$, as well as the respective contributions of the first two modes, $\Psi_{x'}^{(1)}/E'_0$ and $\Psi_{x'}^{(2)}/E'_0$, are compared. Figure 5a shows that the first two modes interact constructively within the narrow gap separating the two nanoparticles, hence leading to a large field enhancement (>10^2) even if we are out of the resonance. Figure 5b and Figure 5c show the spatial distribution of the total electric field, $E'_{x'}/E'_0$, and the contributrion of the first mode, $\Psi_{x'}^{(1)}/E'_0$, respectively. The area where the induced electric field is enhanced compared to the incoming beam amplitude is surrounded by a black dashed line. Whereas the enhancement area spreads outside of the nanowire dimer when only the first mode is considered (Figure 5c), most of the energy is confined within the gap when the total electric field is considered (Figure 5c). The interference between the first two modes is constructive inside the gap but destructive outside, hence leading to a weak radiative coupling. At these invisibility dip frequencies, the nanowire dimer acts as an invisible nanoantenna that can focus light efficiently at the nanoscale without being seen from the far-field. This idea is in relation with the concept of sensor cloaking proposed recently by Alú and Engheta.[55]

Beyond the Quasi-static Limit. Until now, all the theoretical results have been derived under the quasi-static approximation. This is quite restrictive in

perspective of applications since it can only apply to nanostructures of a few tens of nanometers (typically 20 nm). Hence, the conformal transformation approach has to be extended beyond the quasi-static limit by considering the radiative reaction. In the transformed frame, it corresponds to the self-interaction between the dimer and its own scattered field.[56,57] In the slab frame, this radiative reaction corresponds to the field scattered by the fictive absorbers and back-emitted toward the metal slabs.[46] This contribution can be easily derived in the slab geometry, adding the contribution of the absorbing dipoles $\hat{\Delta}_s$ to the expression of the induced electric field $\mathbf{E}(z = 0)$ in eq 12,

$$\mathbf{E}(z = 0) = -\frac{(\hat{\Delta} + \hat{\Delta}_s)}{\pi\varepsilon_0}\beta \quad (24)$$

Replacing $\hat{\Delta}_s$ by its expression (eq 21) in the last equation allows the derivation of a new expression of $\mathbf{E}(z = 0)$ in presence of radiative losses,

$$\mathbf{E}(z = 0) = -\frac{\hat{\Delta}}{\pi\varepsilon_0}\frac{\beta}{1 - i\frac{\pi}{2}g^2{k_o}^2\beta} \quad (25)$$

If we inject this new expression of $\mathbf{E}(z = 0)$ into eq 14, replace $\hat{\Delta}$ (eq 9) and g (eq 5), a new expression for the extinction cross-section can be deduced beyond the quasi-static limit,

$$\sigma_{ext} = 16\pi k_0\rho(\rho+1)D^2\,\mathrm{Im}\left\{\frac{\beta}{1 - i2\pi\rho(1+\rho)D^2{k_o}^2\beta}\right\} \quad (26)$$

By comparing this expression of σ_{ext} with the one derived under the quasi-static approximation (eq 15), one can see that the radiative correction leads to a renormalization of the extinction spectrum by a factor appearing at the denominator of eq 26. The effect of radiative losses has already been investigated in a related work and our approach has been shown to be valid until D_o = 200 nm (see the Figure 3 of ref 13). The radiative damping leads to a saturation of the extinction cross-section at the level of the physical cross-section and also to a broadening of each LSP resonance.

A new expression of the radiated power can also be derived by injecting the new expression of $\mathbf{E}(z = 0)$ (eq 25) into eq 22. Then, after renormalization, a new expression of the scattering cross-section is found beyond the quasi-static limit,

$$\sigma_s = 32\pi^2 k_o^3\rho^2(1+\rho)^2D^4\frac{|\beta|^2}{|1 - i2\pi\rho(1+\rho)D^2{k_o}^2\beta|^2} \quad (27)$$

Radiative damping leads to a renormalization of the scattering cross-section. Whereas a scaling of σ_s^o as D^4 was predicted in the quasi-static limit (eq 23), radiative damping makes the scattering cross-section saturate at the level of the physical cross-section for large structure dimensions, as illustrated by Figure 3 of ref 13.

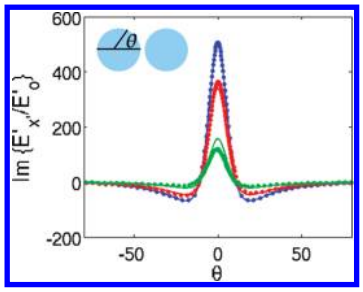

Figure 6. Imaginary part of E'_x/E'_0 along the surface of the nanowire at the first resonant frequency $\omega = 0.8\omega_{sp}$, for ρ = 0.01. The theoretical predictions (continuous lines) and numerical results (dots) are compared for different dimensions: 20 (blue), 50 (red), 100 nm (green).

In the quasi-static limit, the near-field enhancement does not depend on the size of the device. However, radiative damping breaks this property and limits the nanofocusing properties of the dimer. Comparing the expressions of the electric field $\mathbf{E}(z = 0)$ in the slab frame neglecting (eq 12) or considering (eq 25) radiative damping, one can see that the presence of an absorber accounting for radiative losses leads to the renormalization of the emitting dipole $\hat{\Delta}$ by a factor,

$$\eta = 1 - i\frac{\pi}{2}g^2{k_o}^2\beta \quad (28)$$

The same correction can be made in the transformed frame. Radiative reaction requires the renormalization of the electric field by the same factor η. Using eq 5, this factor can be expressed as a function of D

$$\eta = 1 - 2i\pi\rho(1+\rho)D^2k_o^2\beta \quad (29)$$

The effect of the radiative losses on the field enhancement is shown in Figure 6. The imaginary part of E'_x/E'_0 along the surface of the nanowire is displayed at the first resonant frequency $\omega = 0.8\omega_{sp}$ for ρ = 0.01. The theoretical and numerical results are compared for different dimensions D_o = 20, 50, 100 nm, and a good agreement is found. The radiation losses lead to a renormalization of the electric field by the factor η which increases with the structure dimension (eq 29). For D_o = 100 nm, a slight disagreement starts to appear between theory and numerical simulations, due to the retardation effects which are not taken into account by our model.[13]

Figure 7 shows a more systematic investigation of the nanofocusing performance that can provide a nanowire dimer. It shows the maximum field enhancement obtained at the first resonance (eq 16 for $n = 1$) as a function of ρ and D. Note that the maximum field enhancement occurs at the surface of the nanowires, *i.e.*, at $z' = -s$ and $z' = -s - \delta$ (Figure 1). Not surprisingly, the radiative losses make the field enhancement decrease when the structure dimension increases. The white dashed line in Figure 7 corresponds to a gap between the two nanowires of 0.5 nm. This limit is particularly relevant since below it quantum mechanical effects cannot be neglected,[47] and the

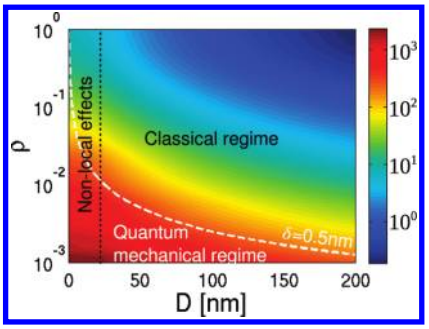

Figure 7. Maximum field enhancement $|E'|/E'_0$ occurring at the first resonance (eq 16, $n = 1$) plotted as a function of the ratio ρ and the cylinder diameter D. The white dashed line represents the region for which the gap δ between the two nanowires is 0.5 nm. The black dashed line corresponds to a 10-nm diameter for the nanowires.

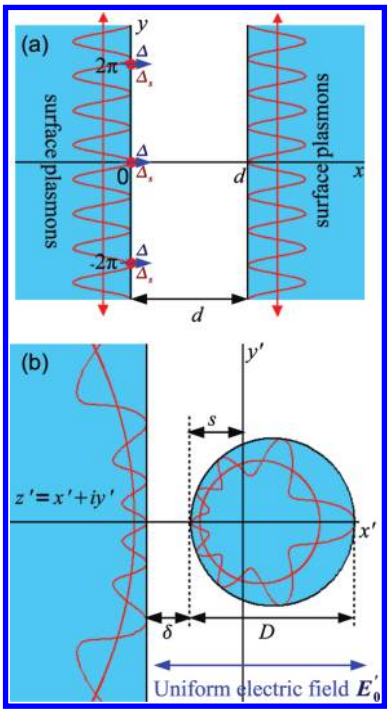

Figure 8. (a) Two semi-infinite metallic slabs separated by a thin dielectric film support surface plasmons that couple to an array of dipoles $\hat{\Delta}$ placed on the insulator−metal interface at $x = 0$. The array pitch is 2π. (b) The transformed material of panel a is a nanowire of diameter D separated by a distance δ from an infinite metal plate. The array of dipoles $\hat{\Delta}$ is transformed into a uniform electric field $\mathbf{E}'_0$.

results of our classical approach may be unrealistic. The black dashed line represents a nanowire diameter of 10 nm. This corresponds to the limit below which nonlocal effects cannot be neglected.[48] Hence, the maximum field enhancement that can be obtained with nanowire dimers is limited to 200 under the classical approach. Larger values correspond to configurations with a gap or a nanowire diameter too small to neglect quantum mechanical or nonlocal effects.

Interaction between a Nanowire and a Metal Plate. The case of a single nanowire placed on top of a metal plate is now investigated. Besides being simpler to implement experimentally than a nanowire dimer, this plasmonic device may provide a better nanofocusing performance. As we will see, the transformation we will use to solve that problem is closely related to the nanowire dimer. Hence, the behavior of surface plasmons is similar in both structures.

Conformal Transformation. The transformation is closely related to the one seen previously for nanowire dimers (see Figure 1). The canonical system is still a metal−insulator−metal structure but the origin of the transformation is now placed at the metal−insulator interface (see Figure 8a). The array of dipoles is also placed infinitely close to this interface. Now, by applying to this system the transformation defined in eq 1, a plasmonic device made of a single nanowire on top of a metal plate is derived. Note that, contrary to the transformation studied in ref 42 in which the nanowire and the metal plate were in contact, there is here a narrow gap separating the nanowire from the metal plate.

Let us first derive all the geometrical parameters of the transformed geometry. The diameter of the cylinder is given by

$$D = \frac{g}{\sinh(d)} \tag{30}$$

The distance δ separating the nanowire from the metal plate can be expressed as

$$\delta = \frac{g}{2}\tanh(d/2) \tag{31}$$

The shift s between the axis y' and the surface of the cylinder is given by

$$s = \frac{g}{1+e^d} \tag{32}$$

We also define a key parameter,

$$\rho' = \frac{\delta}{D} = \sinh^2(d/2) \tag{33}$$

which is the ratio between the gap δ and the cylinder diameter, D. At last, combining eq 30 with eq 33, one can find the expressions of g and d as a function of D and ρ',

$$g = 2D\sqrt{\rho'(1+\rho')} \tag{34}$$

$$d = 2\ln(\sqrt{\rho'} + \sqrt{1+\rho'}) \tag{35}$$

In the transformed geometry, the infiniteness of the metal plate implies a half plane-wave illumination polarized along the x'-axis. In the quasi-static limit, the incident field can be taken as uniform and equal to $\mathbf{E}'_0$ in the dielectric but should vanish in the metal plate. In the slab geometry, this uniform field $\mathbf{E}'_0$ is transformed into a dipolar field for $x > 0$ coming from an array placed along the interface $x = 0$ with a pitch 2π and a strength Δ given by eq 9. On the contrary, the incident field should be zero for $x < 0$. The potential ϕ induced by this half-space illumination in the slab geometry is derived in the Methods section (eqs 72−74).

Absorption Cross-Section of the Nanowire. In the case of a nanowire dimer, the absorption cross-section of the nanostructure was deduced from the electric field induced by the metal slabs at the dipoles in the original frame. Here we wish to compute the absorption cross-section of the nanowire and not of the whole plasmonic system (infinite metal plate + nanowire). Hence the contributions of the electric field coming from the different metal slabs of Figure 8a have to be discriminated. To that aim, the electric field at the dipoles can be decomposed as, $\mathbf{E}(z = 0) = \mathbf{E}^{+}(z = 0) + \mathbf{E}^{-}(z = 0)$, with $\mathbf{E}^{-}$ and $\mathbf{E}^{+}$ the fields coming from the right and the left of Figure 8a, respectively. These two contributions are derived in the Methods section and can be expressed as

$$\mathbf{E}^{\pm}(z = 0) = -\frac{\Delta}{2\pi\varepsilon_0}\beta^{\pm} \tag{36}$$

with

$$\beta^{-} = \frac{\varepsilon - 1}{\varepsilon + 1}\sum_{n=1}^{+\infty}\frac{n}{e^{2nd} - \left(\frac{\varepsilon - 1}{\varepsilon + 1}\right)^2} \quad \text{and}$$

$$\beta^{+} = \frac{\varepsilon - 1}{\varepsilon + 1}\beta^{-} \tag{37}$$

Compared to its expression in the dimer configuration (eq 14), the dipole power dissipated should be divided by 2 due to the half-space illumination:

$$P_{ext} = -\frac{\omega}{4}\mathrm{Im}\{\hat{\Delta}^{*}\cdot\mathbf{E}(z = 0)\} \tag{38}$$

As we want to have access to the power dissipated by the nanowire and not by the whole system, the contribution $\mathbf{E}^{-}(z = 0)$ (eq 36) should be considered instead of the total field $\mathbf{E}(z = 0)$. In the quasi-static limit, the absorption cross-section of the nanowire can then be obtained by normalizing P_{ext} by P_{in}, but the latter quantity should also be divided by 2 compared to its usual value due to the half space illumination: $P_{in} = \varepsilon_o c|E_0'|^2/4$. At last, by replacing $\hat{\Delta}$ by eq 9, g using eq 34, and d using eq 35, the absorption cross-section of the nanowire can be deduced as a function of D and ρ',

$$\sigma_a^o = 8\pi k_0\rho'(1 + \rho')D^2 \times \mathrm{Im}\left\{\frac{\varepsilon - 1}{\varepsilon + 1}\sum_{n=1}^{+\infty}\frac{n}{(\sqrt{\rho'} + \sqrt{1 + \rho'})^{4n} - \left(\frac{\varepsilon - 1}{\varepsilon + 1}\right)^2}\right\} \tag{39}$$

The absorption cross-section is the sum of the contributions due to each surface plasmon mode supported by the system. Each mode may give rise to a resonance at a frequency satisfying the following relation

$$(\sqrt{\rho'} + \sqrt{1 + \rho'})^{4n} = \mathrm{Re}\left\{\left(\frac{\varepsilon - 1}{\varepsilon + 1}\right)^2\right\} \tag{40}$$

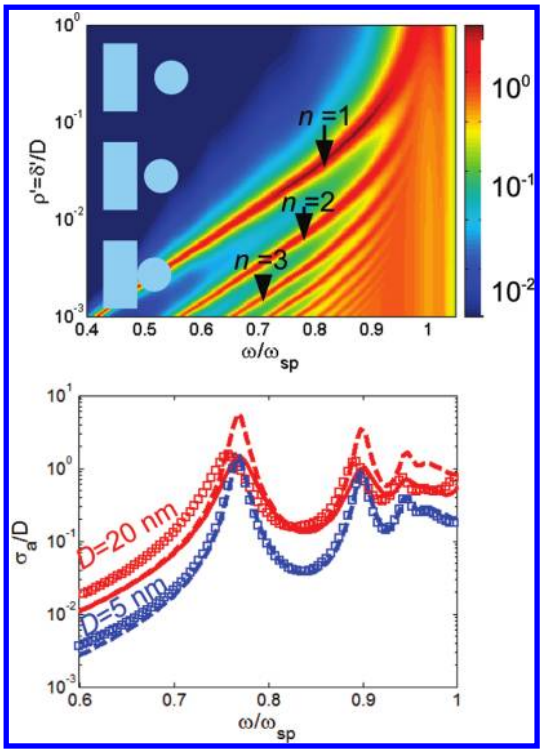

Figure 9. Absorption cross-section σ_a^o normalized by the physical cross-section D for $\rho' = \delta'/D = 0.025$. (a) Dependence in the quasi-static limit as a function of frequency and the ratio $\rho' = \delta'/D$, with $D = 10$ nm. (b) The quasi-static theoretical predictions (dashed lines, eq 39) are compared to numerical simulations (squares) and to the analytical prediction taking into account radiation damping (continuous lines, eq 45) for two cylinder diameters: $D = 5$ nm (blue) and $D = 20$ nm (red).

This condition of resonance only depends on the ratio ρ' between the gap separating the nanowire from the metal plate and the diameter of the nanowire (eq 33). It is worth noting that this relation is slightly different from the one derived for a nanowire dimer (eq 16). Figure 9a displays the absorption cross-section of the nanowire as a function of frequency and the ratio $\rho' = \delta'/D$, for $D = 10$ nm. Similarly to the dimer case, a nanowire placed on top of a metal substrate shows three distinct regimes. For $\delta' > D$ ($\rho' > 1$), the coupling between the metal plate and the nanowire is weak and the absorption cross-section of the nanowire shows only a resonance at $\omega = \omega_{sp}$ similarly to an isolated nanowire. Then, for $\delta' < D$ ($\rho' < 1$), there is an hybridization between the localized surface plasmon supported by the nanowire and the surface plasmon propagating along the metal substrate. Several resonances arise in the visible spectrum, each one being associated to a different angular spectrum. These resonances red-shift when the nanowire approaches the metal substrate. For $\delta' \ll D$ ($\rho' \to 0$), an infinite number of modes are excited, which gives rise to a broadband response, as already studied in ref 42.

Figure 9b shows the comparison of our quasi-static prediction with the results of a numerical simulation.

For $D = 5$ nm, the agreement between the quasi-static theory and numerical simulations is perfect showing the precision of our approach in the quasi-static limit. The confinement of the field in the narrow gap allows the description of the system under the electrostatic approximation even though the system is infinite. On the contrary, for $D = 20$ nm, a discrepancy arises between the quasi-static prediction and the numerical result, due to the radiation losses. Our model should take into account radiation damping to be able to predict properly the optical response of a nanowire of larger dimensions.

Following the same strategy as previously, one can take into account radiative losses by introducing fictive absorbers superimposed to emitting dipoles in the slab geometry. However, the presence of the semi-infinite metal slab has to be considered in the transformed geometry to compute the scattered field. This scattered field $\mathbf{E}'_s$ will be a superposition of the contribution from the dipole moment $\mathbf{p}$ of the nanowire but also from its image relative to the metal plate, by virtue of the theorem of image charges,

$$\mathbf{E}'_s = -i\frac{k^2}{8\varepsilon_o}\mathrm{Re}\left\{1+\frac{\varepsilon-1}{\varepsilon+1}\right\}\mathbf{p} \qquad (41)$$

Note that, as in our previous work,[43] only the imaginary part of the Green function is considered to express the scattered field since its real part does not contribute to the radiative losses. In the slab frame, this uniform field is transformed into an array of small absorbing particles whose dipole moment is given by

$$\hat{\Delta}_s = -i\frac{\pi^2}{2}\varepsilon_o g^2 {k_o}^2 \mathrm{Re}\left\{1+\frac{\varepsilon-1}{\varepsilon+1}\right\}\mathbf{E}(z=0) \qquad (42)$$

To take into account radiative damping, the electric field $\mathbf{E}(z = 0)$ should be rewritten by considering the contribution of $\hat{\Delta}_s$,

$$\mathbf{E}(z=0) = -\frac{(\hat{\Delta}+\hat{\Delta}_s)}{2\pi\varepsilon_0}(\beta^- + \beta^+) \qquad (43)$$

Replacing $\hat{\Delta}_s$ by its expression (eq 42) into the last equation yields

$$\mathbf{E}(z=0) = -\frac{\hat{\Delta}}{2\pi\varepsilon_0}\frac{\beta^- + \beta^+}{1-i\frac{\pi}{4}g^2{k_o}^2\mathrm{Re}\left\{1+\frac{\varepsilon-1}{\varepsilon+1}\right\}(\beta^- + \beta^+)} \qquad (44)$$

This last equation leads to a new expression for the power dissipated by the overall system (eq 38) beyond the quasi-static limit. The scattered power can also be derived using the new expression of $\mathbf{E}(z=0)$: $P_s = -\omega/4\,\mathrm{Im}\{\hat{\Delta}_s^* \cdot \mathbf{E}(z=0)\}$. Then the difference between these quantities yields the overall absorbed

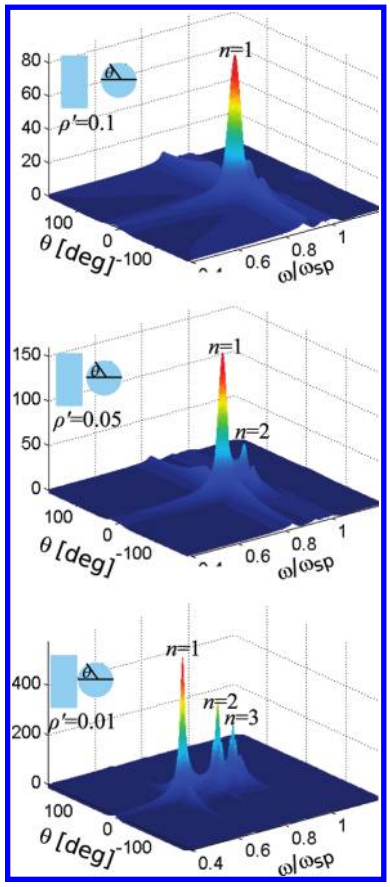

Figure 10. Field enhancement $|E'|/E'_0$ arising at the surface of the nanowire, plotted as a function of the angle θ and frequency, for different values of ρ.

power $P_a = P_{ext} - P_s$,

$$P_a = 2\pi k_0 \varepsilon_0 c|E'_0|^2 \rho'(1+\rho')D^2 \times \frac{\mathrm{Im}\{\beta^+ + \beta^-\}}{\left|1 - i\pi D^2\rho(1+\rho)k_o^2\mathrm{Re}\left\{1+\frac{\varepsilon-1}{\varepsilon+1}\right\}(\beta^- + \beta^+)\right|^2} \qquad (45)$$

The contribution of the nanowire can be extracted from the last equation by only considering the imaginary part of β^- (contribution of $\mathbf{E}^-$) at the numerator of eq 45. A renormalization by the incident power, $P_{in} = \varepsilon_o c|E'_0|^2/4$, leads finally to a new expression of the absorption cross-section, valid beyond the quasi-static limit,

$$\sigma_a = 8\pi k_0 \rho'(1+\rho')D^2 \times \frac{\mathrm{Im}\{\beta^-\}}{\left|1 - i\pi D^2\rho(1+\rho){k_o}^2\left(1+\frac{\varepsilon-1}{\varepsilon+1}\right)(\beta^- + \beta^+)\right|^2} \qquad (46)$$

The comparison of the last equation with the expression of σ_a^o in the quasi-static limit (eq 39) shows that the effect of radiative damping consists in a renormalization by the factor at the denominator of eq 46 which scales as ${k_o}^2D^2$. Figure 9b shows how taking into account radiation

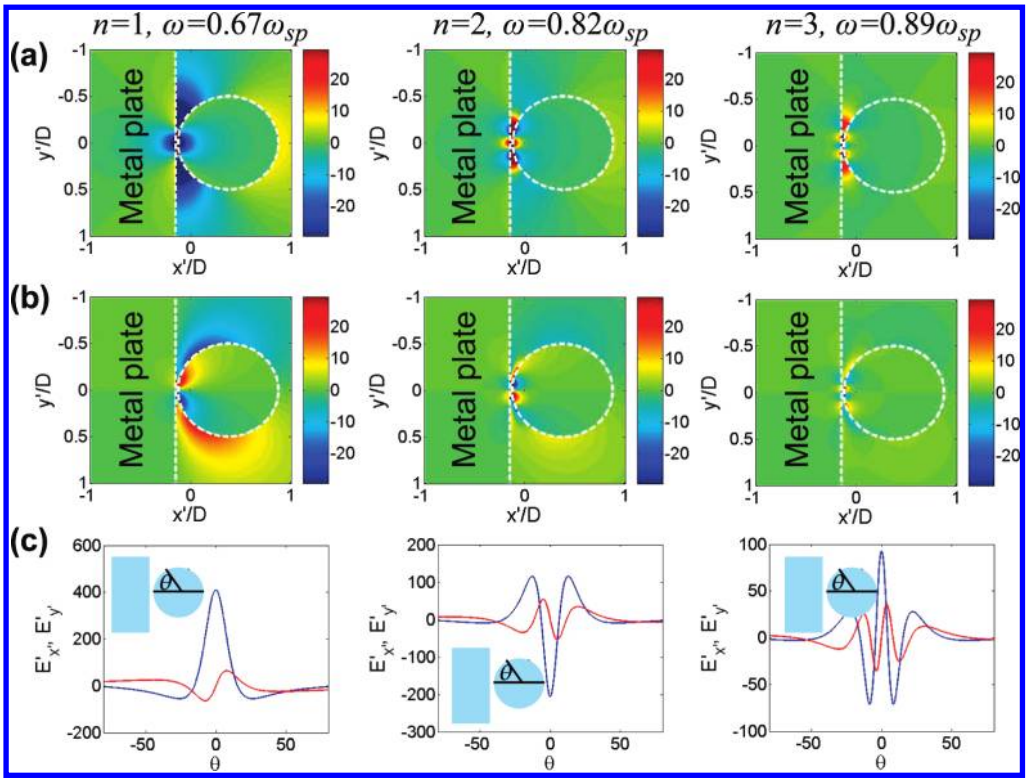

Figure 11. Electric field for $\rho' = 0.01$ associated with the modes n = 1,2,3 (from left to right) at their corresponding resonant frequencies (eq 40). (a) Amplitude of the imaginary part of $\psi_x^{(n)}$ normalized by the incoming field E_0' (polarized along x'). (b) Amplitude of the imaginary part of $\psi_y^{(n)}$ normalized by the incoming field E_0' (polarized along x'). For plots a and b, the color scale is restricted to [−30 30] but note that the field magnitude can be far larger in the narrow gap between the structures. (c) Amplitude of the imaginary part of $\psi_x^{(n)}/E_0'$ (blue) and $\psi_y^{(n)}/E_0'$ (red) along the cylinder surface as a function of the angle θ defined in the figure.

damping can improve the agreement between theory and numerical simulations here for D = 20 nm (see the comparison with the electrostatic result). Nevertheless, a slight disagreement remains and is due to retardation effects which are not taken into account by our model. Note also that, beyond D = 20 nm, our model is no longer sufficient to predict quantitatively the radiative losses.

Electric Field in the Transformed Geometry. The electric field $\mathbf{E}'(x',y')$ in the transformed geometry can be easily deduced from the potential (eqs 17 and 18). Using the expression of the potential ϕ given in eqs 73 and 74, the electric field $\mathbf{E}'$ can be expressed as an infinite sum of modes (eq 19). The analytical expression of the modes $\Psi^{(n)}$ is derived in the Methods section (eqs 76−81).

The resonant feature of these modes is illustrated by Figure 10 which displays the field enhancement, $|E'|/E_0'$, observed along the nanowire surface as a function of the angle θ and frequency for different values of ρ'. At each resonance, the electric field blows up at the nanowire surface, leading to a drastic field enhancement that can be superior to 10^2 for $\rho' \approx 0.01$. Similarly to the dimer case, there is a red-shift of resonances when the nanoparticle approaches the metal surface (*i.e.,* for small values of ρ').

Figure 11 shows the electric field distribution associated with the first three modes taken at their resonant frequencies (eq 40). The gap δ' is fixed to $D/100$ (ρ' = 0.01). The metal is assumed to be silver with permittivity taken from Johnson and Christy.[50] Figure 11 panel sets a and b represent the imaginary part of the field distribution along x' and y', respectively. These figures can be easily interpreted with conformal transformation. In the slab frame, surface plasmon modes transport the energy of the dipoles along the surface of metal slabs (see Figure 8). The same modes are excited in the transformed frame: a SPP propagates along the metal plate and induces a LSP along the nanowire surface. Similarly to the dimer configuration, these two surface plasmons couple to each other in the gap, leading to a drastic field enhancement. However, unlike a nanowire in contact with a metal plate,[42] the velocity of surface plasmons does not vanish and energy cannot accumulate infinitely in the narrow gap. Instead, the SPP continues to propagate along the metal plate without being stopped and the LSP turns around the nanowire indefinitely before being absorbed. This leads to the resonant behavior pointed out previously. Figure 11c represents the imaginary part of the field along the nanowire surface. As for the nanowire dimer, each mode is associated to an angular momentum n which represents the number of spatial periods described by the LSP at each turn around the cylinder. Figure 11c also highlights the drastic field enhancement that can be induced at the surface of the nanowire.

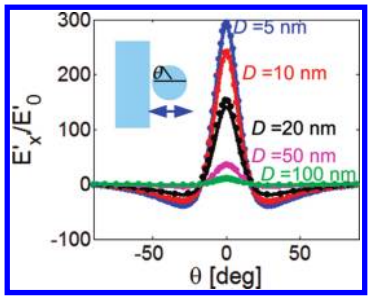

Figure 12. Imaginary part of E'_x/E'_0 along the surface of the nanowire plotted as a function of the angle θ, at the first resonant frequency for $\rho' = 0.025$. The theoretical predictions (continuous lines) and the numerical simulations (dots) are shown for different dimensions (5, 10, 20, 50, 100 nm). Note that, because of retardation effects, the resonances are red-shifted for $D > 5$ nm (see Figure 9b). Hence the numerical results are not shown at the resonant frequency predicted by our theory but at the one observed numerically.

The theoretical expression of the electric field was derived under the quasi-static approximation, which is quite restrictive in terms of applications since radiative losses start to be significant as soon as $D > 5$ nm. As already shown, the effect of radiation damping can be represented by a simple renormalization of the electric field. This factor of normalization can be deduced from the comparison between the expression of the electric field in the original frame, $\mathbf{E}(z = 0)$, with and without considering the radiative losses (eq 36 and eq 43, respectively). It yields the following factor of normalization,

$$\eta = 1 - i\pi\rho(1+\rho)k_o^2 D^2 \mathrm{Re}\left\{1 + \frac{\varepsilon - 1}{\varepsilon + 1}\right\}(\beta^- + \beta^+) \tag{47}$$

Figure 12 compares our theoretical prediction with numerical simulations of the electric field at the first resonance ($n = 1$) along the nanowire for $\rho' = \delta'/D = 0.025$ and for different dimensions. Surprisingly, this agreement is nearly perfect for all dimensions of the nanowire, which demonstrates the power of our approach. Our theory can predict quantitatively the field enhancement reached in the narrow gap separating the nanowire from the metal plate until a nanowire dimension $D = 100$ nm.

CONCLUSION

This article has shown how a transformation optics approach can be a powerful tool to provide an analytical description and a unique physical insight on the propagation of surface plasmons in complex nanostructures. This study has focused on the plasmonic hybridization in the case of nanowire dimers and of a nanowire placed on top of a metal substrate but it can be extended to other configurations such as metallic nanotubes, nanoshells, or 3D dimers.[44] In both cases, we have shown that the interaction between surface plasmons result in several resonances in the visible spectrum which red-shift when the two metallic structures approach each other. Each resonance is associated to a mode characterized by an angular momentum which corresponds to the number of wavelengths displayed by the surface plasmons when propagating one time around each nanoparticle. Invisibility dips have also been pointed out between each of these resonances and result from an interference between each successive mode. This interference is destructive in the far-field of the dimer but constructive in its near-field: these invisibility dips provide a possible path toward the implementation of noninvasive or invisible nanoantenna. Our analytical model predicts quantitatively the optical response as well as the field enhancement induced by these metallic structures within and beyond the quasi-static limit, for nanowire diameters below 100 nm. In practice, this transformation optics strategy can be applied to the optimization of metallic nanostructures. For instance, our analytical approach might be very useful for modeling nonlinear effects such as Raman scattering or fluorescent emission by molecules near metallic nanostructures. As the absorption and emission process occur at different frequencies, a perfect knowledge of the spectral and spatial properties of the field enhancement might be decisive for the implementation of experimental setup aiming at single molecule detection.

METHODS

Nanowire Dimer. The slab problem is first addressed (Figure 1a). The near-field approximation is made, hence we assume that the Laplace's equation is obeyed. Each dipole $\hat{\Delta}$ consists of two line charges. We wish to calculate the potential ϕ induced by the metallic sheets by expanding the incident field ϕ_o of the dipoles as a Fourier series in y:

$$\phi_o(r) = -\frac{1}{2\pi\varepsilon_0}\sum_{n=-\infty}^{n=+\infty}\frac{\hat{\Delta}(\cdot r - 2n\pi)}{|r - 2n\pi|^2} = \frac{1}{2\pi}\int \mathrm{d}k\, \phi_o(k)\, e^{iky} \tag{48}$$

$\phi_o(k)$ can be found by making a Fourier transform in a transverse plane at an arbitrary position x:

$$\phi_o(k) = \int \phi_o(x,y) e^{-iky}\,\mathrm{d}y = \begin{cases} a_+(k)\, e^{-|k|x} & \text{if } x > 0 \\ a_-(k)\, e^{|k|x} & \text{if } x < 0 \end{cases} \tag{49}$$

with

$$a_\pm(k) = \frac{\mp\Delta}{2\varepsilon_0}\sum_{n=-\infty}^{n=+\infty}\delta[k-n] \tag{50}$$

where $\delta[k]$ denotes the Dirac distribution. The incident field is a Dirac comb in the k-space, hence only surface plasmon modes associated to integer spatial frequencies n can be excited.

The next step of our calculation consists in deriving the field $\phi(k)$ induced by the metal plates located in the half planes $x < -d/2$ and $x > d/2$. Because of the odd parity of the incident potential $\phi_0(k)$ and the symmetry of the system, the induced field $\phi(k)$ is also of odd parity. This field can be expressed as follows:

$$\phi(k) = \begin{cases} b(k)\, e^{-|k|x} - b(k)\, e^{|k|x}, & x > -d/2 \text{ and } x < d/2 \\ c(k)\, e^{-|k|x}, & x > d/2 \\ -c(k)\, e^{|k|x}, & x < -d/2 \end{cases} \tag{51}$$

The two unknowns $b(k)$ and $c(k)$ are then determined by the boundary conditions at the metallic slab interfaces,

$$b(k) = -\frac{\Delta}{2\varepsilon_0}\frac{\frac{\varepsilon-1}{\varepsilon+1}}{e^{|k|d}-\frac{\varepsilon-1}{\varepsilon+1}}\sum_{n=-\infty}^{n=+\infty}\delta[k-n] \quad (52)$$

$$c(k) = -\frac{\Delta}{\varepsilon_0(\varepsilon+1)}\frac{e^{|k|d}}{e^{|k|d}-\frac{\varepsilon-1}{\varepsilon+1}}\sum_{n=-\infty}^{n=+\infty}\delta[k-n] \quad (53)$$

An inverse Fourier transform of the induced potential derived in the k-space leads to the solution in the real space,

$$\phi(x,y) = \frac{1}{2\pi}\begin{cases}\int -c(k)\, e^{iky+|k|x}\, dk, & x < -d/2\\ \int -2b(k)\sinh(|k|x)\, e^{iky}\, dk, & |x| < d/2\\ \int c(k)\, e^{iky-|k|x}\, dk, & x > d/2\end{cases} \quad (54)$$

By injecting the expressions of $b(k)$ (eq 52) and $c(k)$ (eq 53), we obtain

$$\phi(|x| < d/2) = \frac{\Delta}{2\pi\varepsilon_0}\frac{\varepsilon-1}{\varepsilon+1}\sum_{n=1}^{+\infty}\frac{\sinh(nz)+\sinh(nz^*)}{e^{nd}-\frac{\varepsilon-1}{\varepsilon+1}} \quad (55)$$

$$\phi(x > d/2) = -\frac{\Delta}{2\pi\varepsilon_0(\varepsilon+1)}\sum_{n=0}^{+\infty}\alpha_n\frac{e^{nd}(e^{-nz}+e^{-nz^*})}{e^{nd}-\frac{\varepsilon-1}{\varepsilon+1}} \quad (56)$$

$$\phi(x < -d/2) = \frac{\Delta}{2\pi\varepsilon_0(\varepsilon+1)}\sum_{n=0}^{+\infty}\alpha_n\frac{e^{nd}(e^{nz}+e^{nz^*})}{e^{nd}-\frac{\varepsilon-1}{\varepsilon+1}} \quad (57)$$

with $\alpha_0 = {}^1/_2$ and $\alpha_{n>0} = 1$. The system here consists of an infinite sum of discrete modes which gives rise to a resonance when $\exp(nd) = \mathrm{Re}[(\varepsilon-1)/(\varepsilon+1)]$. Note that contrary to the case of kissing cylinders for which the induced potential was obtained by directly picking out the pole due to the surface plasmon modes,[12,42] our calculation is here strictly exact and takes into account the contribution of lossy surface waves.[46]

The electric field $\mathbf{E}'(x',y')$ in the transformed geometry can be easily deduced from the potential ϕ (eqs 55−57) using eqs 17−18. It turns out that the electric field can be decomposed as an infinite sum of modes (eq 19). Then, each of these modes $\Psi^{(n)}$ can be expressed in the transformed geometry as a function of D, ρ, and E'_0, replacing $\hat{\Delta}$ by $\mathbf{E}'_0$ (eq 9), d by ρ (eq 4), and g by D and ρ (eq 5):

- For $|z'-D/2+s| > D/2$ and $|z'+D/2+\delta+s| > D/2$ (*i.e.*, outside the cylinders):

$$\psi_{x'}^{(n)} = 2E'_0\rho(1+\rho)D^2\frac{\varepsilon-1}{\varepsilon+1}\frac{n}{(\sqrt{\rho}+\sqrt{1+\rho})^{4n}-\frac{\varepsilon-1}{\varepsilon+1}}\times\left[\frac{1}{z'^2}\left(1+\frac{2\sqrt{\rho(1+\rho)}D}{z'}\right)^{n-1}+\frac{1}{z'^2}\left(1+\frac{2\sqrt{\rho(1+\rho)}D}{z'}\right)^{-n-1}+\frac{1}{z'^{*2}}\left(1+\frac{2\sqrt{\rho(1+\rho)}D}{z'^*}\right)^{n-1}+\frac{1}{z'^{*2}}\left(1+\frac{2\sqrt{\rho(1+\rho)}D}{z'^*}\right)^{-n-1}\right] \quad (58)$$

$$\psi_{y'}^{(n)} = 2iE'_0\rho(1+\rho)D^2\frac{n}{\frac{\varepsilon+1}{\varepsilon-1}(\sqrt{\rho}+\sqrt{1+\rho})^{4n}-1}\times\left[\frac{1}{z'^2}\left(1+\frac{2\sqrt{\rho(1+\rho)}D}{z'}\right)^{n-1}+\frac{1}{z'^2}\left(1+\frac{2\sqrt{\rho(1+\rho)}D}{z'}\right)^{-n-1}-\frac{1}{z'^{*2}}\left(1+\frac{2\sqrt{\rho(1+\rho)}D}{z'^*}\right)^{n-1}-\frac{1}{z'^{*2}}\left(1+\frac{2\sqrt{\rho(1+\rho)}D}{z'^*}\right)^{-n-1}\right] \quad (59)$$

- For $|z'-D/2+s| < D/2$ (*i.e.*, in the cylinder on the right of Figure 1c):

$$\psi_{x'}^{(n)} = \frac{4}{\varepsilon+1}E'_0\rho(1+\rho)D^2\frac{n(\sqrt{\rho}+\sqrt{1+\rho})^{4n}}{(\sqrt{\rho}+\sqrt{1+\rho})^{4n}-\frac{\varepsilon-1}{\varepsilon+1}}\times\left[\frac{1}{z'^2}\left(1+\frac{2\sqrt{\rho(1+\rho)}D}{z'}\right)^{-n-1}+\frac{1}{z'^{*2}}\left(1+\frac{2\sqrt{\rho(1+\rho)}D}{z'^*}\right)^{-n-1}\right] \quad (60)$$

$$\psi_{y'}^{(n)} = i\frac{4}{\varepsilon+1}E'_0\rho(1+\rho)D^2\frac{n(\sqrt{\rho}+\sqrt{1+\rho})^{4n}}{(\sqrt{\rho}+\sqrt{1+\rho})^{4n}-\frac{\varepsilon-1}{\varepsilon+1}}\times\left[\frac{1}{z'^2}\left(1+\frac{2\sqrt{\rho(1+\rho)}D}{z'}\right)^{-n-1}-\frac{1}{z'^{*2}}\left(1+\frac{2\sqrt{\rho(1+\rho)}D}{z'^*}\right)^{-n-1}\right] \quad (61)$$

- For $|z'+D/2+\delta+s| < D/2$ (*i.e.*, in the cylinder on the left of Figure 1c):

$$\psi_{x'}^{(n)} = \frac{4}{\varepsilon+1}E'_0\rho(1+\rho)D^2\frac{n(\sqrt{\rho}+\sqrt{1+\rho})^{4n}}{(\sqrt{\rho}+\sqrt{1+\rho})^{4n}-\frac{\varepsilon-1}{\varepsilon+1}}\times\left[\frac{1}{z'^2}\left(1+\frac{2\sqrt{\rho(1+\rho)}D}{z'}\right)^{n-1}+\frac{1}{z'^{*2}}\left(1+\frac{2\sqrt{\rho(1+\rho)}D}{z'^*}\right)^{n-1}\right] \quad (62)$$

$$\psi_{y'}^{(n)} = i\frac{4}{\varepsilon+1}E'_0\rho(1+\rho)D^2\frac{n(\sqrt{\rho}+\sqrt{1+\rho})^{4n}}{(\sqrt{\rho}+\sqrt{1+\rho})^{4n}-\frac{\varepsilon-1}{\varepsilon+1}}\times\left[\frac{1}{z'^2}\left(1+\frac{2\sqrt{\rho(1+\rho)}D}{z'}\right)^{n-1}-\frac{1}{z'^{*2}}\left(1+\frac{2\sqrt{\rho(1+\rho)}D}{z'^*}\right)^{n-1}\right] \quad (63)$$

Nanowire on Top of a Metal Substrate. As for the nanowire case, the slab problem is first addressed (Figure 8a). Because of the half space illumination, the Fourier component $\phi_o(k)$ of the

incident field in the slab geometry is given by

$$\phi_o(k) = \int \phi_o(x,y)\, e^{-iky}\, dy = \begin{cases} a(k)\, e^{-|k|x} & \text{if } x > 0 \\ 0 & \text{if } x < 0 \end{cases} \quad (64)$$

with

$$a(k) = -\frac{\Delta}{2\varepsilon_0} \sum_{n=-\infty}^{n=+\infty} \delta[k-n] \quad (65)$$

Let us determine the field $\phi(k)$ induced by the metal plates when illuminated by the incident field $\phi_o(k)$ (eq 64). This field can be expressed as follows:

$$\phi(k) = \begin{cases} b_+(k)\, e^{-|k|x} + b_-(k)\, e^{|k|x}, & 0 < x < d \\ c_+(k)\, e^{-|k|x}, & x > d \\ c_-(k)\, e^{|k|x}, & x < 0 \end{cases} \quad (66)$$

The four unknowns $b_+(k)$, $b_-(k)$, $c_+(k)$, and $c_-(k)$ are then determined by the boundary conditions at the metal slab interfaces,

$$b_+(k) = -\frac{\Delta}{2\varepsilon_0}\left(\frac{\varepsilon-1}{\varepsilon+1}\right)^2 \frac{1}{e^{2|k|d} - \left(\frac{\varepsilon-1}{\varepsilon+1}\right)^2} \sum_{n=-\infty}^{n=+\infty} \delta[k-n] \quad (67)$$

$$b_-(k) = \frac{\Delta}{2\varepsilon_0}\frac{\varepsilon-1}{\varepsilon+1} \frac{1}{e^{2|k|d} - \left(\frac{\varepsilon-1}{\varepsilon+1}\right)^2} \sum_{n=-\infty}^{n=+\infty} \delta[k-n] \quad (68)$$

$$c_+(k) = -\frac{\Delta}{\varepsilon_0}\frac{1}{\varepsilon+1} \frac{e^{2|k|d}}{e^{2|k|d} - \left(\frac{\varepsilon-1}{\varepsilon+1}\right)^2} \sum_{n=-\infty}^{n=+\infty} \delta[k-n] \quad (69)$$

$$c_-(k) = \frac{\Delta}{\varepsilon_0}\frac{\varepsilon-1}{(\varepsilon+1)^2} \frac{1}{e^{2|k|d} - \left(\frac{\varepsilon-1}{\varepsilon+1}\right)^2} \sum_{n=-\infty}^{n=+\infty} \delta[k-n] \quad (70)$$

Now that the induced potential is known in the k-space, it can be deduced in the real space *via* an inverse Fourier transform,

$$\phi(x,y) = \frac{1}{2\pi} \begin{cases} \int c_-(k)\, e^{iky+|k|x}\, dk, & x < 0 \\ \int [b_+(k)\, e^{-|k|x} + b_-(k)\, e^{|k|x}]\, e^{iky}\, dk, & 0 < x < d \\ \int c_+(k)\, e^{iky-|k|x}\, dk, & x > d \end{cases} \quad (71)$$

By injecting the expressions of $b_+(k)$ (eq 67), $b_-(k)$ (eq 68), $c_+(k)$ (eq 69), and $c_-(k)$ (eq 70) into the last equation, we obtain

$$\phi(x<0) = \frac{\Delta(\varepsilon-1)}{2\pi\varepsilon_0(\varepsilon+1)^2} \sum_{n=0}^{+\infty} \alpha_n \frac{1}{e^{2nd} - \left(\frac{\varepsilon-1}{\varepsilon+1}\right)^2} [e^{nz} + e^{nz^*}] \quad (72)$$

$$\phi(0<x<d) = \frac{\Delta}{4\pi\varepsilon_0}\frac{\varepsilon-1}{\varepsilon+1} \sum_{n=0}^{+\infty} \frac{\alpha_n}{e^{2nd} - \left(\frac{\varepsilon-1}{\varepsilon+1}\right)^2} \times \left[-\frac{\varepsilon-1}{\varepsilon+1}(e^{-nz} + e^{-nz^*}) + (e^{nz} + e^{nz^*})\right] \quad (73)$$

$$\phi(x>d) = -\frac{\Delta}{2\pi\varepsilon_0}\frac{1}{\varepsilon+1} \sum_{n=0}^{+\infty} \alpha_n \frac{e^{2nd}}{e^{2nd} - \left(\frac{\varepsilon-1}{\varepsilon+1}\right)^2} (e^{-nz} + e^{-nz^*}) \quad (74)$$

As previously, our problem here consists of an infinite sum of discrete modes which gives rise to a resonance when $\exp(2nd) = \mathrm{Re}[(\varepsilon-1)^2/(\varepsilon+1)^2]$. Now that the slab problem is solved, we can deduce the solution in the transformed frame.

In the case of a nanowire dimer, the absorption cross-section of the nanostructure was deduced from the electric field induced by the metal slabs at the dipoles in the original frame. Here we wish to compute the absorption cross-section of the nanowire and not of the whole plasmonic system (infinite metal plate + nanowire). Hence the contributions of the electric field coming from the different metal slabs of Figure 8a have to be discriminated. The electrostatic potential between these two slabs (eq 73) can be decomposed as

$$\phi(0<x<d) = \phi^- + \phi^+, \quad \text{with}$$

$$\phi^\pm = \frac{1}{2\pi}\int b_\pm(k)\, e^{|k|x}\, e^{iky}\, dk \quad (75)$$

ϕ^- and ϕ^+ correspond to the field coming from the right and the left of Figure 8a, respectively. Their counterpart in the transformed geometry (Figure 8b) will represent the contribution coming from the nanowire and the metal plate, respectively. The electric field at the dipoles can be decomposed in a similar way, $\mathbf{E}(z=0) = \mathbf{E}^+(z=0) + \mathbf{E}^-(z=0)$, with $\mathbf{E}^\pm = -\nabla\phi^\pm$. Using the expressions of $b_\pm(k)$ (eq 67−68), the potentials $\phi^\pm$ can be deduced (eq 75) and their gradients yield the expressions for $\mathbf{E}^\pm(z=0)$ given in eq 36.

The electric field $\mathbf{E}'(x',y')$ in the transformed geometry can be easily deduced from the potential ϕ (eqs 72−74) using eqs 17 and 18. It turns out that the electric field $\mathbf{E}'$ can be expressed as an infinite sum of modes (eq 19). Each mode $\Psi^{(n)}$ can be expressed in the transformed geometry as a function of D, ρ', and E'_o, replacing $\hat{\Delta}$ by $\mathbf{E}'_0$ (eq 9), d by ρ (eq 33), and g by D and ρ' (eq 34):

- For $x' < -(s+\delta)$ (*i.e.*, in the metal plate):

$$\psi^{(n)}_{x'} = \frac{4n\rho'(1+\rho')D^2E_0(\varepsilon-1)}{(\varepsilon+1)^2} \times \frac{1}{(\sqrt{\rho'}+\sqrt{1+\rho'})^{4n} - \left(\frac{\varepsilon-1}{\varepsilon+1}\right)^2} \times \left[\frac{1}{z'^2}\left(1+\frac{2\sqrt{\rho'(1+\rho')}D}{z'}\right)^{n-1} + \frac{1}{z'^{*2}}\left(1+\frac{2\sqrt{\rho'(1+\rho')}D}{z'^*}\right)^{n-1}\right] \quad (76)$$

$$\psi^{(n)}_{y'} = i\frac{4n\rho'(1+\rho')D^2E_0(\varepsilon-1)}{(\varepsilon+1)^2} \times \frac{1}{(\sqrt{\rho'}+\sqrt{1+\rho'})^{4n} - \left(\frac{\varepsilon-1}{\varepsilon+1}\right)^2} \times \left[\frac{1}{z'^2}\left(1+\frac{2\sqrt{\rho'(1+\rho')}D}{z'}\right)^{n-1} - \frac{1}{z'^{*2}}\left(1+\frac{2\sqrt{\rho'(1+\rho')}D}{z'^*}\right)^{n-1}\right] \quad (77)$$

- For $x' > -(s + \delta)$ and $|z' - D/2 + s| > D/2$ (*i.e.*, in the dielectric):

$$\psi_{x'}^{(n)} = 2E_0\rho'(1+\rho')D^2\frac{\varepsilon-1}{\varepsilon+1}\frac{n}{(\sqrt{\rho'}+\sqrt{1+\rho'})^{4n}-\left(\frac{\varepsilon-1}{\varepsilon+1}\right)^2}$$
$$\times\left\{\frac{\varepsilon-1}{\varepsilon+1}\left[\frac{1}{z'^2}\left(1+\frac{2\sqrt{\rho'(1+\rho')}D}{z'}\right)^{-n-1}+\frac{1}{z'^{*2}}\left(1+\frac{2\sqrt{\rho'(1+\rho')}D}{z'^*}\right)^{-n-1}\right]+\left[\frac{1}{z'^2}\left(1+\frac{2\sqrt{\rho'(1+\rho')}D}{z'}\right)^{n-1}+\frac{1}{z'^{*2}}\left(1+\frac{2\sqrt{\rho'(1+\rho')}D}{z'^*}\right)^{n-1}\right]\right\} \quad (78)$$

$$\psi_{y'}^{(n)} = \mathrm{i}2E_0\rho'(1+\rho')D^2\frac{\varepsilon-1}{\varepsilon+1}\frac{n}{(\sqrt{\rho'}+\sqrt{1+\rho'})^{4n}-\left(\frac{\varepsilon-1}{\varepsilon+1}\right)^2}$$
$$\times\left\{\frac{\varepsilon-1}{\varepsilon+1}\left[\frac{1}{z'^2}\left(1+\frac{2\sqrt{\rho'(1+\rho')}D}{z'}\right)^{-n-1}-\frac{1}{z'^{*2}}\left(1+\frac{2\sqrt{\rho'(1+\rho')}D}{z'^*}\right)^{-n-1}\right]+\left[\frac{1}{z'^2}\left(1+\frac{2\sqrt{\rho'(1+\rho')}D}{z'}\right)^{n-1}-\frac{1}{z'^{*2}}\left(1+\frac{2\sqrt{\rho'(1+\rho')}D}{z'^*}\right)^{n-1}\right]\right\} \quad (79)$$

- For $|z' - D/2 + s| < D/2$ (*i.e.*, in the nanowire):

$$\psi_{x'}^{(n)} = 4E_0\rho'(1+\rho')D^2\frac{1}{\varepsilon+1}\frac{n(\sqrt{\rho'}+\sqrt{1+\rho'})^{4n}}{(\sqrt{\rho'}+\sqrt{1+\rho'})^{4n}-\left(\frac{\varepsilon-1}{\varepsilon+1}\right)^2}$$
$$\times\left[\frac{1}{z'^2}\left(1+\frac{2\sqrt{\rho'(1+\rho')}D}{z'}\right)^{-n-1}+\frac{1}{z'^{*2}}\left(1+\frac{2\sqrt{\rho'(1+\rho')}D}{z'^*}\right)^{-n-1}\right] \quad (80)$$

$$\psi_{y'}^{(n)} = \mathrm{i}4E_0\rho'(1+\rho')D^2\frac{1}{\varepsilon+1}\frac{n(\sqrt{\rho'}+\sqrt{1+\rho'})^{4n}}{(\sqrt{\rho'}+\sqrt{1+\rho'})^{4n}-\left(\frac{\varepsilon-1}{\varepsilon+1}\right)^2}$$
$$\times\left[\frac{1}{z'^2}\left(1+\frac{2\sqrt{\rho'(1+\rho')}D}{z'}\right)^{-n-1}-\frac{1}{z'^{*2}}\left(1+\frac{2\sqrt{\rho'(1+\rho')}D}{z'^*}\right)^{-n-1}\right] \quad (81)$$

Acknowledgment. The authors would like to thank Y. Luo and A. I. Fernández-Domínguez for fruitful discussions. This work was supported by the European Community project PHOME (Contract No. 213390) and by the UK Engineering and Physical Sciences Research Council (EPSRC).

REFERENCES AND NOTES

1. Ebbesen, T. W.; Lezec, H. J.; Ghaemi, H. F.; Thio, L.; Wolff, P. A. Extraordinary Optical Transmission Through Small Apertures. *Nature* **1998,** *391*, 667–669.
2. Pendry, J. B. Negative Refraction Makes a Perfect Lens. *Phys. Rev. Lett.* **2000,** *85*, 3966–3969.
3. Barnes, W. L.; Dereux, A.; Ebbesen, T. W. Surface Plasmon Subwavelength Optics. *Nature* **2003,** *424*, 824–830.
4. Bozhevolnyi, S. I.; Volkov, V. S.; Devaux, E.; Laluet, J.-Y.; Ebbesen, T. W. Channel Plasmon Subwavelength Waveguide Components Including Interferometers and Ring Resonators. *Nature* **2006,** *440*, 508–511.
5. Nie, S.; Emory, S. Probing Single Molecules and Single Nanoparticles by Surface-Enhanced Raman Scattering. *Science* **1997,** *275*, 1102–1106.
6. Kneipp, K.; Wang, Y.; Kneipp, H.; Perelman, L.; Itzkan, I.; Dasari, R.; Feld, M. Single Molecule Detection Using Surface-Enhanced Raman Scattering (SERS). *Phys. Rev. Lett.* **1997,** *78*, 1667–1670.
7. Dulkeith, E.; Morteani, A. C.; Niedereichholz, T.; Klar, T. A.; Feldmann, J.; Levi, S. A.; van Veggel, F. C. J. M.; Reinhoudt, D. N.; Moller, M.; Gittins, D. I. Fluorescence Quenching of Dye Molecules near Gold Nanoparticles: Radiative and Nonradiative Effects. *Phys. Rev. Lett.* **2002,** *89*, 203002.
8. Kuhn, S.; Hakanson, U.; Rogobete, L.; Sandoghdar, V. Enhancement of Single-Molecule Fluorescence Using a Gold Nanoparticle. *Phys. Rev. Lett.* **2006,** *97*, 017402.
9. Kim, S.; Jin, J.; Kim, Y. J.; Park, I. Y.; Kim, Y.; Kim, S. High-Harmonic Generation by Resonant Plasmon Field Enhancement. *Nature* **2008,** *453*, 757–760.
10. Hao, E.; Schatz, G. Electromagnetic Fields Around Silver Nanoparticles and Dimers. *J. Chem. Phys.* **2003,** *120*, 357–366.
11. Kelly, K. L.; Coronado, E.; Zhao, L. L.; Schatz, G. C. The Optical Properties of Metal Nanoparticles: The Influence of Size, Shape, and Dielectric Environment. *J. Phys. Chem. B* **2003,** *107*, 668–677.
12. Aubry, A.; Lei, D. Y.; Fernández-Domínguez, A. I.; Sonnefraud, Y.; Maier, S. A.; Pendry, J. B. Plasmonic Light Harvesting Devices Over the Whole Visible Spectrum. *Nano Lett.* **2010,** *10*, 2574–2579.
13. Aubry, A.; Lei, D. Y.; Maier, S. A.; Pendry, J. B. Interaction between Plasmonic Nanoparticles Revisited with Transformation Optics. *Phys. Rev. Lett.* **2010,** *105*, 233901.
14. Akimov, A. V.; Mukherjee, A.; Yu, C. L.; Chang, D. E.; Zibrov, A. S.; Hemmer, P. R.; Park, H.; Lukin, M. D. Generation of Single Optical Plasmons in Metallic Nanowires Coupled to Quantum Dots. *Nature* **2007,** *450*, 402–406.
15. Lee, H. W.; Schmidt, M. A.; Tyagi, H. K.; Sempere, L. P.; Russell, P. S. J. Polarization-Dependent Coupling to Plasmon Modes on Submicron Gold Wire in Photonic Crystal Fiber. *Appl. Phys. Lett.* **2008,** *93*, 111102.
16. Oulton, R. F.; Sorger, V. J.; Zentgraf, T.; Ma, R.-M.; Gladden, C.; Dai, L.; Bartal, G.; Zhang, X. Plasmon Lasers at Deep Subwavelength Scale. *Nature* **2009,** *461*, 629–632.
17. Hill, R. T.; Mock, J. J.; Urzhumov, Y.; Sebba, D. S.; Oldenburg, S. J.; Chen, S.-Y.; Lazarides, A. A.; Chilkoti, A.; Smith, D. R. Highly Confined Electromagnetic Fields in Arrays of Strongly Coupled Ag Nanoparticles. *Nano Lett.* **2010,** *10*, 4150–4154.
18. Bergman, D. J. Dielectric Constant of a Two-Component Granular Composite: A Practical Scheme for Calculating the Pole Spectrum. *Phys. Rev. B* **1979,** *19*, 2359–2378.
19. Bergman, D. J. The Dielectric Constant of a Simple Cubic Array of Identical Spheres. *J. Phys. C: Solid State Phys.* **1979,** *12*, 4947–4960.
20. Bergman, D. J. Theory of Resonances in the Electromagnetic Scattering by Macroscopic Bodies. *Phys. Rev. B* **1980,** *22*, 3527–3539.
21. McPhedran, R. C.; Kenzie, D. R. M. Electrostatic and Optical Resonances of Arrays of Cylinders. *Appl. Phys.* **1980,** *23*, 223–235.
22. McPhedran, R.; Perrins, W. Electrostatic and Optical Resonances of Cylinder Pairs. *Appl. Phys.* **1981,** *24*, 311–318.
23. Schmeits, M.; Dambly, L. Fast Electron Scattering by Bispherical Plasmon Modes. *Phys. Rev. B* **1991,** *44*, 12706–12712.

24. Kottmann, J.; Martin, O. Plasmon Resonant Coupling in Metallic Nanowires. *Opt. Exp.* **2001,** *8*, 655–663.
25. Rechberger, W.; Hohenau, A.; Leitner, A.; Krenn, J. R.; Lamprecht, B.; Aussenegg, F. R. Optical Properties of Two Interacting Gold Nanoparticles. *Opt. Commun.* **2003,** *220*, 137–141.
26. Su, K.-H.; Wei, Q.-H.; Zhang, X.; Mock, J. J.; Smith, D. R.; Schultz, S. Interparticle Coupling Effects on Plasmon Resonances of Nanogold Particles. *Nano Lett.* **2003,** *3*, 1087–1090.
27. Atay, T.; Song, J.-H.; Nurmikko, V. Strongly Interacting Plasmon Nanoparticle Pairs: From Dipole−Dipole Interaction to Conductively Coupled Regime. *Nano Lett.* **2004,** *4*, 1627–1631.
28. Romero, I.; Aizpurua, J.; Bryant, G.; de Abajo, F. G. Plasmons in Nearly Touching Metallic Nanoparticles. *Opt. Exp.* **2006,** *14*, 9988–9999.
29. Giannini, V.; Sánchez-Gil, J. A. Calculations of Light Scattering from Isolated and Interacting Metallic Nanowires of Arbitrary Cross-Section by Means of Green's Theorem Surface Integral Equations in Parametric Form. *J. Opt. Soc. Am. A* **2007,** *24*, 2822–2830.
30. Lassiter, J. B.; Aizpurua, J.; Hernandez, L.; Brandl, D.; Romero, I.; Lal, S.; Hafner, J.; Nordlander, P.; Halas, N. Close Encounters between Two Nanoshells. *Nano Lett.* **2008,** *8*, 1212–1218.
31. Funston, A. M.; Novo, C.; Davis, T. J.; Mulvaney, P. Plasmon Coupling of Gold Nanorods at Short Distances and in Different Geometries. *Nano Lett.* **2009,** *9*, 1651–1658.
32. Xu, H.; Käll, M. Surface-Plasmon-Enhanced Optical Forces in Silver Nanoaggregates. *Phys. Rev. Lett.* **2002,** *89*, 246802.
33. Li, K.; Stockman, M. I.; Bergman, D. J. Self-Similar Chain of Metal Nanospheres as an Efficient Nanolens. *Phys. Rev. Lett.* **2003,** *91*, 227402.
34. Genov, D. A.; Sarychev, A. K.; Shalaev, V. M.; Wei, A. Resonant Field Enhancements from Metal Nanoparticle Arrays. *Nano Lett.* **2004,** *4*, 153–158.
35. Sweatlock, L.; Maier, S.; Atwater, H.; Penninkhof, J.; Polman, A. Highly Confined Electromagnetic Fields in Arrays of Strongly Coupled Ag Nanoparticles. *Phys. Rev. B* **2005,** *71*, 235408.
36. Prodan, E.; Radloff, C.; Halas, N. J.; Nordlander, P. A Hybridization Model for the Plasmon Response of Complex Nanostructures. *Science* **2003,** *302*, 419–422.
37. Nordlander, P.; Oubre, C.; Prodan, E.; Li, K.; Stockman, M. Plasmon Hybridization in Nanoparticle Dimers. *Nano Lett.* **2004,** *4*, 899–903.
38. Nordlander, P.; Prodan, E. Plasmon Hybridization in Nanoparticles Near Metallic Surfaces. *Nano Lett.* **2004,** *4*, 2209–2213.
39. Jain, P. K.; Eustis, S.; El-Sayed, M. A. Plasmon Coupling in Nanorod Assemblies: Optical Absorption, Discrete Dipole Approximation Simulation, and Exciton-Coupling Model. *J. Phys. Chem. B* **2006,** *110*, 18243–18253.
40. Moradi, A. Plasmon Hybridization in Metallic Nanotubes. *J. Phys. Chem Sol* **2008,** *69*, 2936–2938.
41. Luo, Y.; Pendry, J.; Aubry, A. Surface Plasmons and Singularities. *Nano Lett.* **2010,** *10*, 4186–4191.
42. Lei, D. Y.; Aubry, A.; Maier, S. A.; Pendry, J. B. Broadband Nano-Focusing of Light Using Kissing Nanowires. *New J. Phys.* **2010,** *12*, 093030.
43. Aubry, A.; Lei, D. Y.; Maier, S. A.; Pendry, J. B. A Broadband Plasmonic Device Concentrating the Energy at the Nanoscale: The Crescent-Shaped Cylinder. *Phys. Rev. B* **2010,** *82*, 125430.
44. Fernández-Domínguez, A. I.; Maier, S. A.; Pendry, J. B. Collection and Concentration of Light by Touching Spheres: A Transformation Optics Approach. *Phys. Rev. Lett.* **2010,** *105*, 266807.
45. Lei, D. Y.; Aubry, A.; Luo, Y.; Maier, S. A.; Pendry, J. B. Plasmonic Interaction between Overlapping Nanowires. *ACS Nano* **2011,** *5*, 597–607.
46. Aubry, A.; Lei, D. Y.; Maier, S. A.; Pendry, J. B. Conformal Transformation Applied to Plasmonics Beyond the Quasistatic Limit. *Phys. Rev. B* **2010,** *82*, 205109.
47. Zuloaga, J.; Prodan, E.; Nordlander, P. Quantum Description of the Plasmon Resonances of a Nanoparticle Dimer. *Nano Lett.* **2009,** *9*, 887–891.
48. McMahon, J. M.; Gray, S. K.; Schatz, G. C. Optical Properties of Nanowire Dimers with a Spatially Nonlocal Dielectric Function. *Nano Lett.* **2010,** *10*, 3473–3481.
49. García-Vidal, F.; Pendry, J. Collective Theory of Surface Enhanced Raman Scattering. *Phys. Rev. Lett.* **1996,** *77*, 1163–1166.
50. Johnson, P. B.; Christy, R. Optical Constants of the Noble Metals. *Phys. Rev. B* **1972,** *6*, 4370–4379.
51. Hao, F.; Sonnefraud, Y.; Dorpe, P. V.; Maier, S. A.; Halas, N. J.; Nordlander, P. Symmetry Breaking in Plasmonic Nanocavities: Subradiant LSPR Sensing and a Tunable Fano Resonance. *Nano Lett.* **2008,** *8*, 3983–3988.
52. Zhang, S.; Genov, D. A.; Wang, Y.; Liu, M.; Zhang, X. Plasmon-Induced Transparency in Metamaterials. *Phys. Rev. Lett.* **2008,** *101*, 047401.
53. Verellen, N.; Sonnefraud, Y.; Sobhani, H.; Hao, F.; Moshchalkov, V. V.; Dorpe, P. V.; Nordlander, P.; Maier, S. A. Fano Resonances in Individual Coherent Plasmonic Nanocavities. *Nano Lett.* **2009,** *9*, 1663–1667.
54. Liu, N.; Langguth, L.; Weiss, T.; Kastel, J.; Fleischhauer, M.; Pfau, T.; Nordlander, P.; Giessen, H. Plasmonic Analogue of Electromagnetically Induced Transparency at the Drude Damping Limit. *Nat. Mater.* **2009,** *8*, 758–762.
55. Alú, A.; Engheta, N. Cloaking a Sensor. *Phys. Rev. Lett.* **2009,** *102*, 233901.
56. Wokaun, A.; Gordon, J. P.; Liao, P. F. Radiation Damping in Surface Enhanced Raman Scattering. *Phys. Rev. Lett.* **1982,** *48*, 957–960.
57. Draine, B. T. The Discrete-Dipole Approximation and Its Application to Interstellar Graphite Grains. *Astrophys. J.* **1988,** *333*, 848–872.